

## Coupling a Local Elastic Solver to a Background Acoustic Model to Estimate Phase Variation

Bram Willemsen, M.I.T., Alison Malcolm, Memorial University

### SUMMARY

In characterizing reservoirs, we are often interested in detailed elastic parameters about only a very limited part of the subsurface. To that end, we introduce a local solver which uses an acoustic solver to propagate the wavefield to a sub-domain on which we use a local elastic solver. This avoids the use of an expensive full domain elastic solver while still incorporating elastic physics in the region where it is most important. We apply the local solver to modeling phase variation with angle.

### INTRODUCTION

The Finite Difference (FD) modeling of seismic waves is an essential component in workflows such as wave equation migration and Full Waveform Inversion. As the most computationally intensive component of these workflows, any increase in its efficiency will have a major impact. Therefore a lot of research is conducted on the process of speeding up the computation, see for instance the work of Wang et al. (2011) and Zepeda-Núñez and Demanet (2016). One particular way to speed up the computation of the finite difference simulation is by using local solvers. They reduce the size of the computational domain to a smaller region of interest by first performing several full domain simulations in a pre-computation step. Broadly speaking, local solvers can be subdivided into exact local solvers (van Manen et al., 2007; Willemsen et al., 2016) and inexact local solvers. By relaxing accuracy constraints, the inexact local solvers attain higher computational efficiency. The inexact elastic local solver formulation of for instance Robertsson and Chapman (2000) allows the model to be perturbed within the local domain. Computational gains are achieved by discarding waves scattering from these perturbations, exiting the local domain, scattering in the inhomogeneous background model and subsequently reentering the local domain.

Primary reflections are waves that by their very nature reflect only once. They therefore do not reenter a local domain centered around a reflector and are accurately modeled by this local solver, and thus modeling primary reflections with this type of inexact local solver will not result in significant accuracy loss. A P-wave reflecting as a P-wave is called a PP reflection. The reflection coefficient of such a primary PP reflection depends on the contrast in the P-wave velocity, density and S-wave velocity along an interface (Červený and Hron, 1961). The critical incidence angle of the incident wave is the angle at which the transmitted wave propagates parallel to the interface. The critical incidence angle marks the transition to reflections with large amplitude and phase shift as described by the Zoeppritz equations for an incoming plane wave. The characteristics of this phase shift depend on the contrast in elastic properties along the interface. Observations made by Zhu and McMechan (2012) suggest that this phase shift is stable dur-

ing propagation through the overburden. This is contrasted by the amplitude of the reflection which reduces at each interface in the overburden due to transmission losses. This makes phase-variation with angle (PVA) a useful quantity to determine material properties at an interface. Recent work (Zhu and McMechan, 2012, 2014) uses these phase shifts to invert for material parameters along the interface. An essential component for such an inversion is to have an efficient forward model. In this paper, we modify the elastic local solver of Robertsson and Chapman (2000) for this purpose. We use the observation that the overburden has little effect on the phase of the propagating wave to reduce the required precomputation by using an acoustic solver for the scalar wave equation.

### METHODOLOGY

The local solver used in this study is a modification of the local solver introduced by Robertsson and Chapman (2000). This local solver generates an approximation of the scattered field due to a model perturbation within the local domain. The only component of the wavefield discarded by the local solver is the wavefield scattering on the perturbation, leaving the local domain, and then scattering on the perturbation again before being recorded by the receivers (i.e. some multiples). The local solver requires background Green's functions between the sources and the receivers, between the sources and the boundary of the local domain and finally those between the receivers and the boundary of the local domain. Figure 1 gives a graphical representation of the local domain in relation to the full domain. A single source and receiver are shown with a star and triangle respectively. The sources and receivers are located in a white box representing the full domain. The pink box surrounding the full domain represents the Perfectly Matched Layer (PML) boundary conditions, although free surface boundary conditions are allowed as well. The gray lines represent the aforementioned background Green's functions connecting the sources and receivers to each other and to the injection/recording boundary of the local solver represented by the red box. The local solver is surrounded by PML boundary conditions. This local PML is typically only a fraction the full domain one.

In order to decouple the local solver from the full domain, a large number of full domain Green's functions need to be computed first. Elastic full domain simulations are inherently more expensive than constant density acoustic (CDA) simulations. Computing the large number of required background Green's functions in an elastic medium may be impractically expensive. In certain applications, such as the computation of PVA of a PP reflection, the elastic behavior is primarily needed at the reflection point. As motivated by observations of Zhu and McMechan (2012), the phase of the PP reflection is stable while the PP reflection travels through the weakly layered elastic overburden. If we use an efficient scalar CDA solver

## A mixed acoustic-elastic local solver

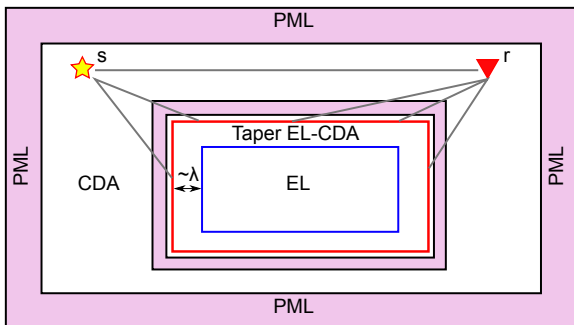


Figure 1: Schematic of the local solver. The different components are explained in the methodology section.

instead of an elastic (EL) solver to propagate the wavefield through the overburden, the observed phase is expected to be similar. The elastic material parameters are most important at the reflection point, where their contrasts determine the phase shift of the postcritical reflection.

This motivates the following computational simplification for the local solver. We define the background state as CDA and compute the associated background Green's functions using the scalar CDA solver from the numerical code PySIT. The boundary integral along the red box in Figure 1 therefore uses the standard CDA form

$$p^{sc}(y,t) = \int_S \left[ G_0(x,y,t) * \frac{\partial p(x,t)}{\partial x_n} - p(x,t) * \frac{\partial G_0(x,y,t)}{\partial x_n} \right] dS_x, \quad (1)$$

where  $*$  is convolution and the surface integral is over coordinate  $x$ .  $G_0(x,y,t)$  is the background CDA Green's function between boundary position  $x$  and evaluation position  $y$ . The boundary integral propagates to the receiver positions  $y$  any scattered field generated by a perturbation added to the background model within the red box. To model the PVA of an elastic reflection we add to the background P-velocity model the density and S-velocity model in the red box of Figure 1. The region between the blue and the red boxes has size proportional to the dominant wavelength and is used to taper the EL model in the blue box to the CDA model at the red box and the background model outside of it. An elastic research code is used to simulate the wavefield in the interior of the local solver (Levander, 1988). Equation 1 will then propagate this wavefield to the receiver locations. Both the elastic code and the CDA code are 4-th order accurate in space, although the formulation naturally extends to higher order of accuracy. With this formulation we are only required to use the elastic solver on a subset of the full domain and never on the entire domain. In the following section we demonstrate the capability of the local solver to model PVA on a synthetic geological model resembling a North Sea field.

## RESULTS

Figure 2 displays a P-wave velocity model resembling a typical North Sea geology. The top 80m of the model represent

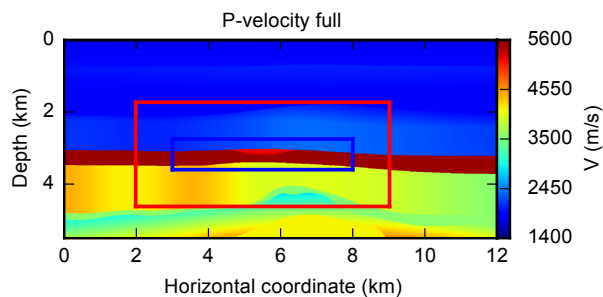


Figure 2: P-wave velocity model resembling a typical North Sea geology. The red and blue boxes are described in the methodology section.

the shallow North Sea. The next 3 kilometers consists of layers slowly increasing in P-velocity with depth. Below these layers a very high velocity layer is present, representing chalk. At a horizontal coordinate of 5.5 km there is a small decrease in velocity due to the presence of hydrocarbons. From this P-velocity model we derive a density model and an S-velocity model for the rock using Gardner's equation and assuming a Poisson solid respectively. This combination of P-velocity, density and S-velocity models represents the True Earth for our purposes. On this Earth model we observe very strong postcritical reflections, because the large increase in P-velocity at the boundary of the chalk layer gives rise to a small critical incidence angle.

In order to compare the phase shift from the full domain elastic simulation with that from the local solver we first compute the required background Green's functions using the efficient CDA solver. We then taper the density and S-velocity model as described above. The results are displayed in Figure 3. The density and S-velocity in the blue box are equal to the true Earth model. The density is tapered to a constant value of 2100.0 and the S-velocity is tapered to 0.0 as required by CDA propagation outside the red box. This way the spatial variation in these density and S-velocity models is restricted to the interior domain of the local solver, with constant values outside. The density and S-velocity models in Figure 3 are the perturbations to the P-velocity only background model. The scattered field from these perturbations is propagated to the receiver locations using equation 1. It is then added to the background wavefield at the receiver, which is obtained by convolving the background Green's function between the source and receiver with the 6.0 Hz Ricker source wavelet. The sum of the background and scattered wavefield is the perturbed wavefield.

Figure 4 shows four different shotgathers for a source at  $x=2.5$  km. The sources and receivers are placed in the water layer at a depth of 10.0 m. The top panel shows the full domain elastic simulation on the true P-velocity, density and S-velocity models. The event marked by the number 1 is the top-of-reservoir reflection. Following this event to larger offsets we first see the head-wave separating from reflection at position 2. This indicates that we are beyond the critical angle. The phase of the reflection at the position marked by the number 3 is almost reversed compared to position 1, with a gradual change hap-

### A mixed acoustic-elastic local solver

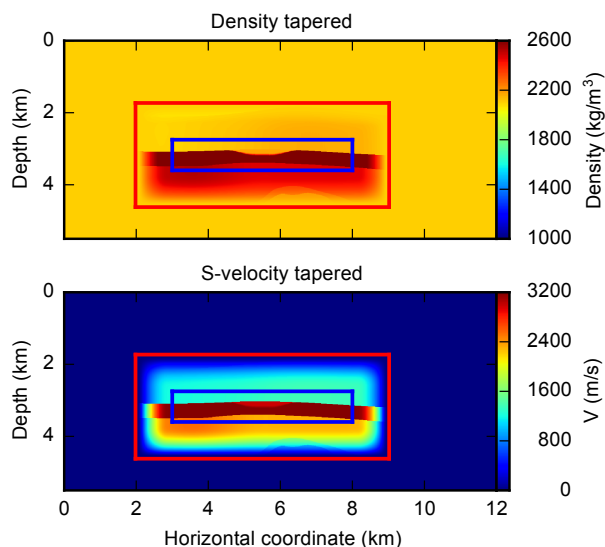


Figure 3: The density and S-wave velocity are tapered outwards from the blue box towards a CDA state with S-velocity 0.0 at the red box.

pening in-between these positions. The second panel of Figure 4 shows the result of using the elastic full domain solver on the P-velocity model of Figure 2 and the tapered density and S-velocity models of Figure 3. Even though the density and S-velocity models are very different outside of the red box, the phase of the top-of-reservoir reflection is quite similar to the simulation on the true Earth model in the first panel. The third panel uses the local elastic solver in combination with the cheap CDA Green's functions in the same model as is used in the second panel. If the background CDA Green's functions are correctly coupled to the elastic local solver, the third panel should be exactly the same as the second panel. The final panel shows a full domain simulation on the pure P-velocity model of Figure 2. It is easy to see that this P-velocity model does not correctly model the phase-shift we observe on the elastic true Earth model. This clearly demonstrates the need to have an elastic propagator to model these events.

For a source at  $x=2.5\text{km}$  and a receiver at  $x=8.5\text{km}$ , the reflection point is at the hydrocarbon-bearing anticline at  $x=5.5\text{km}$ . The phase shift therefore contains valuable information about the elastic contrast at this interface (Červený and Hron, 1961), making accurate modeling important. Figure 5 shows traces corresponding to the four panels in Figure 4 at a receiver coordinate of  $x=8.5\text{km}$ . The full domain simulation on the true Earth model is represented by the black line. The full domain simulation using the padded density and S-velocity models is represented by the blue line. The red line of the local solver simulation is right on top of it, demonstrating its correct implementation. Finally the green line is the P-velocity only result. Note that the amplitude of the true Earth simulation is the lowest of all. One reason is that the nonzero S-velocity allows the energy of the incoming P-wave to reflect as both S-waves and P-waves at each overburden interface, reducing the energy propagating to the chalk layer. The density is also

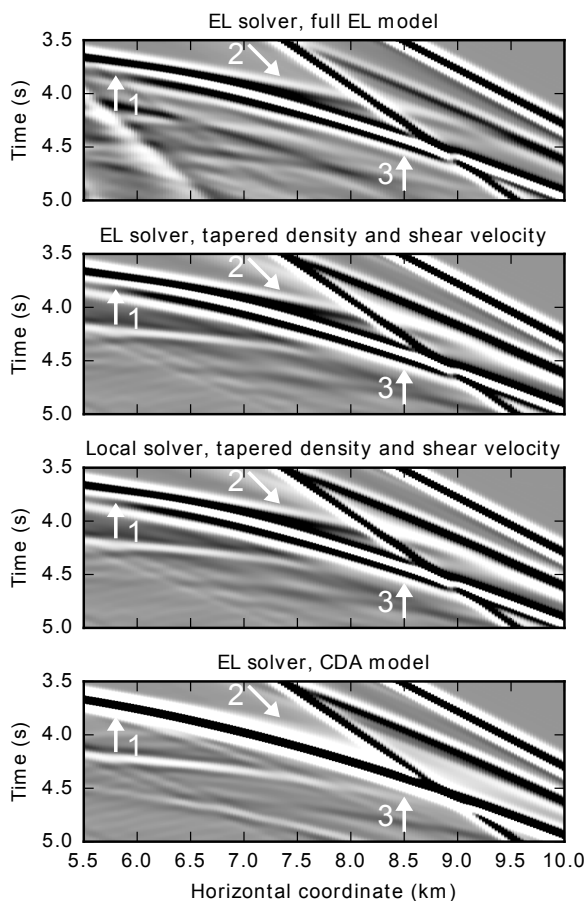


Figure 4: Sections of shotgathers for a source at  $x=2.5\text{km}$  in four different scenarios. The horizontal axis is the receiver coordinate. Three different locations of interest are marked. 1: The top of reservoir reflection. 2: The head-wave separating from this reflection, marking the transition to the post-critical regime. 3: The phase of the top-of-reservoir reflection is obviously shifted compared to position 1 in the first three panels.

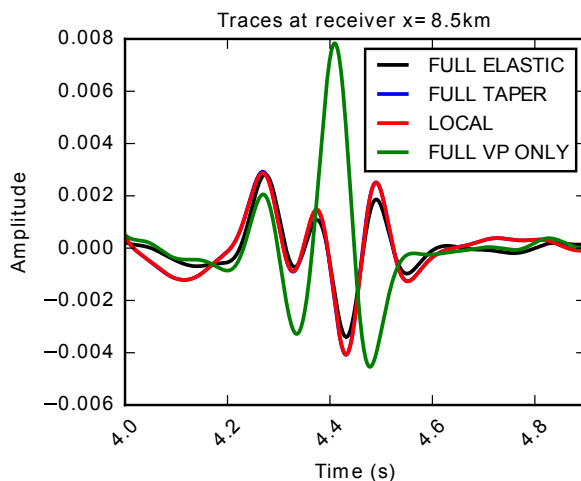


Figure 5: Traces corresponding to the four scenarios in Figure 4 in the same order at  $x=8.5\text{km}$  marked by the number 3 in the first panel. The red line almost perfectly matches the blue line.

## A mixed acoustic-elastic local solver

proportional to the P-velocity through Gardner's equation, resulting in larger impedance contrasts compared to a constant density scenario and a further reduction in energy. Because of this the amplitude of the true Earth reflection at 4.4 s is different than the local solver estimate by about 20 percent, but the phase appears to match quite well. The P-velocity only simulation in green is obviously inadequate with a phase mismatch close to 180 degrees (sign reversal). Its amplitude is also very incorrect due to the simplified representation of the Earth.

### DISCUSSION

The local solver introduced in this paper efficiently models phase shift due to local elastic material contrasts. An efficient forward model is an essential tool in an inversion strategy where phase variation with angle is used to invert for material parameters at the reservoir, because many forward models are needed to find the model which best matches the observed field data. A local solver could be particularly useful in a time-lapse study. If physical changes are restricted to the local domain, the Green's functions never need to be recomputed. They can therefore be reused in the next repeat survey.

The local solver we introduce avoids the high cost of full domain elastic solves by using acoustic Green's functions to propagate the wavefield to the location where the elastic interactions matter most. Only in this region is the expensive elastic solver then used, substantially reducing the computational cost of the procedure. The number of nodes in the local solver is approximately one-fifth of that in the full domain, including PML nodes. As a result the speedup over the full domain solver is only a factor of 5 in this example. The example used in this paper uses an unnecessarily large local domain if the reflection on the hydrocarbon reservoir is the only event of interest. This is done to easily visualize the capability of the formulation to accurately model post-critical phase-shift over a large offset range as is displayed in Figure 4. Higher speedup factors are obtained by shrinking the domain to a smaller size. In a 3D setting the number of nodes reduces more drastically compared to the full domain due to the extra dimension. A higher frequency wavelet may also allow for a thinner taper.

A straight-forward way to increase the speed of the local solver is to exploit the limited residence time of the PP reflection within the local domain. The CDA Green's functions propagate the waves from the source to the local domain and from the local domain to the receivers. The local solver only needs to compute the time in-between. A smaller local domain and a narrower wavelet increase the potential savings from this procedure by reducing the reflections' residence time.

The current model tapers the S-velocity towards 0, which is a large contrast to the S-velocity within the blue box. As a result the taper zone has to be quite large, putting a lower bound on the speedup factor that can be obtained. Future work will focus on tapering the S-velocity to a non-zero constant value. We will investigate the possibility of injecting the acoustic wavefield obtained from the CDA solver on a material with non-zero shear velocity by appropriately scaling it in a way consistent

with the elastic formulation of the local solver. The acoustic boundary integral will no longer pick up the entire scattered field, since it is insensitive to the scattered S-waves. Future research will be needed to verify that the P-reflection will still be propagated correctly. If there is no longer a need to taper the S-velocity to zero, the taper zone is expected to shrink significantly, further improving the speed of the local solver.

If a good full domain density model is available, Variable Density Acoustic (VDA) background Green's functions can naturally replace their CDA equivalents. A density taper would no longer be necessary within the local solver, potentially allowing for a smaller local domain and consequently resulting in local solves with higher speed. The VDA equivalent of the boundary integral in equation 1 would include a density term. If the application justifies the cost of computing expensive full domain elastic background Green's functions, no taper zones would be necessary at all anymore. In this scenario a lot of offline work is done generating the Green's functions, with the benefit of no longer needing any tapers because both the local and full domain simulations use the same physics. The local domain now shrinks to the blue box, dramatically speeding up the local solves. The value of the full domain elastic Green's functions is correlated to the accuracy with which the elastic model parameters are known outside of the region of interest.

In this paper we only visually inspect the agreement between the local solver with CDA Green's functions and the elastic full domain simulation. More work is needed to quantify any potential discrepancies between the phase predicted by this local solver and the full domain simulation. Any such discrepancies would vanish if the elastic Green's functions would be used.

The local solver can be extended to include attenuation as is discussed in Robertsson and Chapman (2000). This can be important since attenuation causes dispersion and can consequently change the shape of the wavelet.

### CONCLUSIONS

With the exception of reentering scattered waves, the local solver introduced in this paper models exactly the wavefield in an elastic medium embedded in a fluid. The use of a full domain elastic solver is avoided. In this paper we applied the solver to Phase Variation with Angle (PVA). Due to the general nature of the formulation, the local solver could be used to efficiently model other phenomena where elastic behavior is most important in a restricted region.

### ACKNOWLEDGEMENTS

We thank Filippo Brogini for insightful discussions. This work is supported by Chevron and with grants from the Natural Sciences and Engineering Research Council of Canada Industrial Research Chair Program and the Research and Development Corporation of Newfoundland and Labrador and by the Hibernia Management and Development Corporation. We would also thank MIT and the ERL consortium members for their support.

## EDITED REFERENCES

Note: This reference list is a copyedited version of the reference list submitted by the author. Reference lists for the 2016 SEG Technical Program Expanded Abstracts have been copyedited so that references provided with the online metadata for each paper will achieve a high degree of linking to cited sources that appear on the Web.

## REFERENCES

- Červený, V., and F. Hron, 1961, Reflection coefficients for spherical waves: *Studia Geophysica et Geodaetica*, **5**, 122–132, <http://dx.doi.org/10.1007/BF02585356>.
- Levander, A. R., 1988, Fourth-order finite-difference p-sv seismograms: *Geophysics*, **53**, 1425–1436, <http://dx.doi.org/10.1190/1.1442422>.
- Robertsson, J., and C. Chapman, 2000, An efficient method for calculating finite-difference seismograms after model alterations: *Geophysics*, **65**, 907–918, <http://dx.doi.org/10.1190/1.1444787>.
- van Manen, D.-J., J. O. A. Robertsson, and A. Curtis, 2007, Exact wave field simulation for finite-volume scattering problems: *The Journal of the Acoustical Society of America*, **122**, EL115–EL121, <http://dx.doi.org/10.1121/1.2771371>.
- Wang, S., M. V. de Hoop, and J. Xia, 2011, On 3d modeling of seismic wave propagation via a structured parallel multifrontal direct Helmholtz solver: *Geophysical Prospecting*, **59**, 857–873, <http://dx.doi.org/10.1111/j.1365-2478.2011.00982.x>.
- Willemsen, B., A. Malcolm, and W. Lewis, 2016, A numerically exact local solver applied to salt boundary inversion in seismic full-waveform inversion: *Geophysical Journal International*, **204**, 1703–1720, <http://dx.doi.org/10.1093/gji/ggv547>.
- Zepeda-Núñez, L., and L. Demanet, 2016, The method of polarized traces for the 2d Helmholtz equation: *Journal of Computational Physics*, **308**, 347–388, <http://dx.doi.org/10.1016/j.jcp.2015.11.040>.
- Zhu, X., and G. A. McMechan, 2012, Elastic inversion of near- and postcritical reflections using phase variation with angle: *Geophysics*, **77**, no. 4, R149–R159, <http://dx.doi.org/10.1190/geo2011-0230.1>.
- Zhu, X., and G. A. McMechan, 2014, Amplitude and phase versus angle for elastic wide-angle reflections in the  $\tau$ -p domain: *Geophysics*, **80**, no. 1, N1–N9, <http://dx.doi.org/10.1190/geo2013-0191.1>.